

High- p_T suppression and elliptic flow from radiative energy loss with realistic bulk medium expansion

Denes Molnar and Deke Sun

Physics Department, Purdue University, West Lafayette, IN 47907

(Dated: October 18, 2018)

We investigate nuclear suppression and elliptic flow in $A+A$ reactions using Gyulassy-Levai-Vitev (GLV) radiative energy loss with the covariant transport MPC for bulk medium evolution. At both RHIC and LHC energies, we find that inclusion of realistic transverse expansion for the medium strongly suppresses elliptic flow at high p_T compared to calculations with longitudinal Bjorken expansion only. We argue that this is a generic feature of GLV energy loss. Transverse expansion also enhances the high- p_T suppression, while fluctuations in energy loss with the rescattering location of the jet parton in the medium lead to weaker suppression and smaller elliptic flow. However, unlike the strong reduction of elliptic flow with transverse expansion, these latter effects get nearly washed out once calculations are adjusted to reproduce R_{AA} in central collisions.

PACS numbers: 12.38.Mh, 24.85.+p, 25.75-q

I. INTRODUCTION

Understanding parton energy loss in ultrarelativistic heavy-ion reactions has been the focus of considerable recent theoretical effort. A variety of phenomenological approaches (e.g., [1–3]) formulate the problem deterministically, in terms of a local energy loss rate $dE/dL = -f(E(L), T(L), L)$ that depends on local temperature, position, and parton energy along the Eikonal (straight-line) parton trajectory. In the weak-coupling regime, more rigorous treatment is possible based on perturbative QCD[4–6]. This includes quantum interference effects and also fluctuations, namely, energy loss for a given jet becomes a stochastic variable that is a function of the scattering and emission history of the jet.

A critical step in computing heavy-ion observables from any energy loss model is spatial and temporal averaging over the bulk medium formed in the collision. We employ here the Gyulassy-Levai-Vitev (GLV) framework[6] in which a high-energy parton loses energy through gluon radiation induced by interactions with static Yukawa scatterers in the medium. It was natural for us to combine this approach with parton transport for the bulk evolution, namely Molnar’s Parton Cascade[7] (MPC). Selected early findings were highlighted in [8]. Here we present a comprehensive set of results from a numerically improved calculation.

Our approach is similar to recent work by Buzzatti and Gyulassy[9] or Horowitz[10], but with a few key differences. Unlike [9], we only focus here on light partons, and do not include multiple gluon radiation, elastic energy loss, or energy loss fluctuations due to variations in radiated gluon momentum. However, as in [8], we *do* include medium evolution with realistic 3D expansion, both longitudinal and transverse, which turns out to crucially influence elliptic flow and also affect the nuclear suppression factor. We also study how differences between deterministic (average) energy loss and stochastic energy loss, which fluctuates depending on where the jet parton interacts with the medium, impact observables.

Recent assessment by the PHENIX Collaboration[11] highlighted the difficulty perturbative QCD parton energy loss frameworks have with reproducing nuclear suppression at RHIC as a function of the angle with the reaction plane, $R_{AA}(\phi)$. GLV calculations were noticeably absent from that analysis but our work here provides a very similar cross-check of the GLV framework. The two observables we study, azimuthally averaged (traditional) R_{AA} and elliptic flow v_2 , carry essentially the same information[32] as $R_{AA}(\phi)$.

II. INGREDIENTS OF THE CALCULATION

A. Energy loss framework

We consider here the Gyulassy-Levai-Vitev (GLV) formulation of energy loss[6], which provides the spectrum of gluons radiated by a jet parton as an expansion in the total number of scatterings n the jet and the radiated gluon experience with the medium as they travel through it. The dominant contribution is given by the leading $n = 1$ (single scattering) term

$$x \frac{dN^{(1)}}{dx d^2\mathbf{k}} = \frac{C_R \alpha_s}{\pi^2} \chi \int d^2\mathbf{q} \frac{\mu^2(z)}{\pi[\mathbf{q}^2 + \mu^2(z)]^2} \frac{2\mathbf{k}\mathbf{q}}{\mathbf{k}^2(\mathbf{k} - \mathbf{q})^2} \times \left(1 - \cos \frac{(\mathbf{k} - \mathbf{q})^2 z}{2xE} \right). \quad (1)$$

Here, x and \mathbf{k} are the light-cone momentum fraction and transverse momentum of the radiated gluon, the jet energy is E , the original hard scattering is at $z = 0$, the jet is moving in the z direction and rescatters once at position z , $\mu(z)$ is the local Debye screening mass, $\chi = \int dz \rho \sigma$ is the opacity for *gluon* jets (irrespective of the jet Casimir C_R), and $\sigma = 9\pi\alpha_s^2/(2\mu^2)$ is the (screened) total $gg \rightarrow gg$ scattering cross section provided the medium is made of gluons. The result was obtained for a medium of static Yukawa scatterers that are well-separated with mean distance $d \gg 1/\mu$, the radiated

gluon is assumed to be soft ($x \ll 1$), and the calculation was done at tree level. Higher-order terms in number of scatterings have been systematically investigated[12], up to at least $n = 9$, and were found to give modest corrections to the $n = 1$ result.

We integrate the spectrum (1) numerically to obtain a momentum-averaged energy loss

$$\Delta E^{(1)}(z) = \int dx d^2\mathbf{k} E x \frac{dN^{(1)}}{dx d^2\mathbf{k}} \quad (2)$$

for *fixed* z , i.e., retain energy loss fluctuations due to variations in z only. The probability for the scattering to occur at z is

$$p(z) = \frac{\rho(z)\sigma(z)}{\chi}. \quad (3)$$

Integrating over z as well yields the deterministic average energy loss

$$\langle \Delta E^{(1)} \rangle = \int dz p(z) \Delta E^{(1)}(z). \quad (4)$$

For asymptotic jet energies, the average energy loss (4) is given by the GLV “pocket formula” [13]

$$\langle \Delta E^{(1)} \rangle \approx \frac{9\pi C_R \alpha_s^3}{4} \int dz z \rho(z) \ln \frac{2E}{\mu^2 z} \quad (5)$$

Though this remarkably compact expression (and its even simpler cousin without the $\ln[2E/(\mu^2 z)]$ factor) has motivated workers in the past, it is unreliable in practice even for qualitative conclusions. Basic constraints that i) the radiated gluon energy does not exceed the energy of the parent jet, ii) momentum transfer in scattering off a thermal particle in the medium has *on average* an upper bound given by the center-of-mass energy available, and iii) the radiated gluon energy must exceed the plasma frequency for the gluon to propagate in the medium, translate into kinematic bounds

$$k < xE, \quad q < \sqrt{6ET}, \quad xE \gtrsim \mu, \quad (6)$$

and lead to (see App. A)

$$\Delta E^{(1)}(z) = \frac{2C_R \alpha_s}{\pi} E \chi I\left(b = \frac{z}{\tau(z)}, \epsilon = \frac{E}{\mu(z)}\right) \quad (7)$$

where $\tau(z) = 2E/\mu^2(z)$ is a characteristic formation time, and the function I is determined by the integral (A2). For small $b \rightarrow 0$ and large $E/\mu \rightarrow \infty$, $I(b, E/\mu \rightarrow \infty) \approx -(\pi/2)b \ln b$, and one recovers (5). However, as shown in Fig. 1, the pocket formula does not account for smaller energy energy loss for less energetic jets, and it also shows a peculiar maximum and turnover at higher z/τ .

Jet and medium parameters enter only through the arguments of I , which simplifies the calculation considerably because we can precalculate a 2D table and interpolate later. Tabulating I is still time consuming because

the integrand is oscillatory. To speed up the numerics, in [8] we used the approximate expression (A6) that involves one fewer integrals. Here we use the full result (A2) and confirm in Fig. 1 the accuracy of our earlier calculation (thin dotted lines).

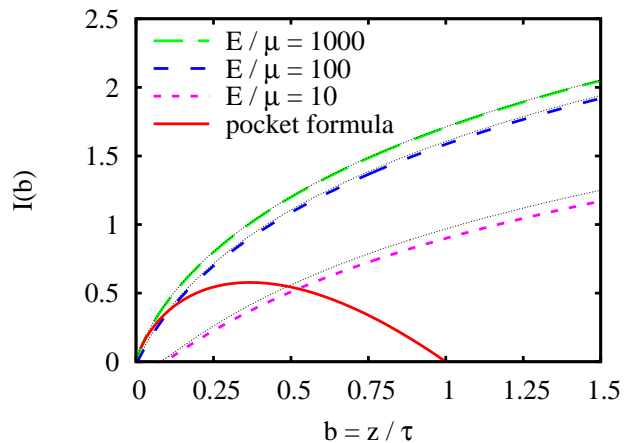


FIG. 1: Function $I(b, E/\mu)$ that governs GLV energy loss $\Delta E(z)$ in this work (see text). Simple analytic “pocket formula” (solid line) valid for asymptotic jet energies and small z/τ is compared to the result with kinematic cutoffs (dashed lines) for various jet energies. Thin dotted lines are for an approximate calculation of I in our earlier work [8].

For very small $b \approx 0$, I can go slightly negative, implying a small energy gain instead of energy loss. In the calculation we cut these off and set $I = 0$ whenever negative contributions arise (see, e.g., the curve for $E/\mu = 10$ below $b < 0.1$ in Fig. 1).

We emphasize that here we only consider radiative energy loss as encoded in (1). There are significant additional contributions from collisional energy loss[14]. Recoil of scattering centers in scattering also enhances[15] energy loss because it effectively changes the denominator $(\mathbf{q}^2 + \mu^2)^2$ in (1) to $\mathbf{q}^2(\mathbf{q}^2 + \mu^2)$. One also expects potentially large higher-order corrections in the strong coupling constant α_s that are yet to be computed. In our approach all these effects get roughly incorporated into the parameter α_s when we calibrate the calculation to a subset of observables through $\Delta E \sim \alpha_s^3$. Equivalently, throughout this paper we apply (1) with *rescaled* opacities $\chi \rightarrow Z\chi$ with scaling factor $Z = 3$ (i.e., $\Delta E \sim Z\alpha_s^3$).

B. Coupling to bulk medium

Coupling energy loss to bulk medium evolution involves several open questions and assumptions (see, e.g., [16] and references therein for a detailed discussion). First, the GLV result (1) was derived for a medium of *static* scattering centers whereas in a heavy-ion collision the density changes rapidly with time. Unfortunately, the formulation has not been extended yet to

time-dependent background color fields. Therefore, as is customary in practice, for *non-static* media we reinterpret $\rho(z)$ in the GLV formula as the local density $\rho(z, t = t_0 + z)$ along the parton trajectory.

Second, it is nontrivial to apply perturbative energy loss unless the medium is also perturbative. For example, questions arise whether the scatterers are quark- or gluon-like quasiparticles or some other field configurations, and whether the key parameter in (1), the local Debye mass $\mu \sim gT$, is computed from the temperature ($\sim T$), local energy density ($\sim e^{1/4}$), or some other thermodynamic quantity. For simplicity, we will consider here the medium to be a system of massless gluons that thermalize to a large degree by Bjorken proper time $\tau_0 = 0.6$ fm. The local $\mu(z)$ is then determined along the straight-line jet path from the local temperature, which we calculate using tabulated density evolution $n(\mathbf{x}_\perp, \eta = 0, \tau)$ from the bulk dynamics model. For our gluon gas, $n \approx 2T^3$ and $\mu = gT \approx 2T$ (similar expressions have been used in [13]). We set aside the interesting question of quark chemical equilibration, namely, how quark/antiquark abundances build up after the early gluon-dominated stage of the collision. At fixed parton density, quarks would significantly lower the opacity because of their smaller Casimir C_2 . (On the other hand, the Debye mass would only be affected by $\sim 10\%$ based on perturbation theory[33].)

Another open question is energy loss prior to the assumed thermalization time τ_0 . Reference [9] found GLV energy loss to be quite sensitive to whether density for $\tau < \tau_0$ was taken to be constant, or rising linearly with τ , or zero. However, differences in early density evolution were largely compensated by slightly different values of α_s when the calculation was calibrated to experimental data. We assume here at early times $\tau < \tau_0$ a linear density build-up $\rho(\mathbf{x}_\perp, \eta, \tau) = \tau\rho(\mathbf{x}_\perp, \eta, \tau_0)/\tau_0$.

One also has to address energy loss in the low-temperature (hadronic) regime, where the isolated Yukawa scattering center assumption in GLV clearly breaks down. In the calculation here we do not include hadrons, and simply set vanishing $\Delta E(z) = 0$ for jet path sections where $\mu < \Lambda_{QCD}$, with cutoff $\Lambda_{QCD} = 0.2$ GeV.

Though we expect that our qualitative conclusions are robust, it would be interesting to vary the assumptions above in the future.

C. Jet initial conditions and fragmentation

We take initial jet momentum distributions in p+p, Au+Au and Pb+Pb from leading-order (LO) perturbative QCD with one-loop running coupling $\alpha_s(Q^2)$, using CTEQ5L parton distribution function parameterizations[17] with $Q^2 = p_{T,parton}^2$. Nuclear effects such as shadowing are ignored but isospin (proton-neutron difference) is included. We consider jets produced at midrapidity both in coordinate and momentum space, i.e., $y = \eta = 0$, where y and η are the coordi-

nate and momentum rapidity[34]. The jet transverse momentum distribution is generated uniformly in azimuth, while the transverse density distribution follows the binary collision distribution for two Woods-Saxon distributions $\rho_A(r)$. I.e., for collisions with impact parameter b we use the transverse profile

$$\frac{dN(\mathbf{b})}{d^2\mathbf{x}_\perp} = const \times T_A\left(\mathbf{x}_\perp + \frac{\mathbf{b}}{2}\right) T_A\left(\mathbf{x}_\perp - \frac{\mathbf{b}}{2}\right), \quad (8)$$

where $T_A(\mathbf{b}) \equiv \int dz \rho_A(\sqrt{z^2 + \mathbf{b}^2})$ is the nuclear thickness function. Woods-Saxon parameters for gold and lead nuclei were taken from HIJING[18]. To enhance statistics at high p_T , we generate uniform jet p_T in the intervals [2, 80] GeV for RHIC and [2, 300] GeV for LHC, and then appropriately reweight contributions to reflect the real jet spectrum.

The density evolution of scatterers is calculated as discussed in the next Section. After energy loss, jets are fragmented independently using LO BKK95 fragmentation function parameterizations[19] with scale factor $Q^2 = p_{T,hadron}^2$, and we take $\pi_0 = (\pi^+ + \pi^-)/2$ for the neutral pion yield. This procedure reproduces high- p_T π_0 and charged particle spectra in p+p at RHIC and LHC with a modest K -factor $K_{NLO} \approx 2.5$ to account for higher-order contributions.

D. Bulk medium evolution for $\tau > \tau_0$

For medium evolution *without* transverse expansion, we use the initial conditions discussed later in this Section but keep the transverse profile “frozen”, i.e., as in [9, 10], the local density undergoes longitudinal Bjorken expansion $\rho(\mathbf{x}_\perp, \eta, \tau) = \rho(\mathbf{x}_\perp, \eta, \tau_0)\tau_0/\tau$.

For medium evolution *with* transverse expansion, we employ covariant transport theory in the same spirit as Refs. [20, 21] to model the collective expansion of a causal, relativistic, low-viscosity bulk medium. We evolve a system of massless “gluons” with $2 \rightarrow 2$ interactions via MPC[7] (Molnar’s Parton Cascade), i.e., solve

$$p_1^\mu \partial_\mu f_1 = S(x, \mathbf{p}_1) + \iiint_{234} (f_3 f_4 - f_1 f_2) W_{12 \rightarrow 34} \times \delta^4(p_1 + p_2 - p_3 - p_4). \quad (9)$$

Here the integrals are shorthands for $\int_i \equiv \int d^3 p_i / (2E_i)$, and $f_j \equiv f(x, \mathbf{p}_j)$ is the phase space density. The source function S specifies the initial conditions, while $W = (1/\pi) s^2 d\sigma/dt$ controls the local scattering rate.

We use isotropic $d\sigma/dt = 2\sigma_{tot}/s$, for simplicity, with $\sigma_{tot}(\tau) = \sigma_0(\tau/\tau_0)^{2/3}$ growing with time so that the shear viscosity to entropy ratio η/s stays approximately constant[21, 22]. To generate substantial elliptic flow $v_2(p_T \approx 3 \text{ GeV}) \sim 0.25$ in collisions with $b = 8$ fm impact parameter at RHIC and LHC, we set $\sigma_0 = 8$ mb and 4.5 mb respectively.

Initial conditions for Au+Au at $\sqrt{s_{NN}} = 200$ GeV and Pb+Pb at $\sqrt{s_{NN}} = 2.76$ TeV with impact parameter $b = 3$ and 8 fm (about 0-10% and 30% centrality, respectively) are constructed as follows. As in [20], we start at proper time $\tau_0 = 0.6$ fm with a locally thermalized system at temperature $T = 0.385$ GeV. Because we are only interested in observables at midrapidity, we set up longitudinally boost invariant conditions in a wide coordinate rapidity window $|\eta| < 5$, with rapidity densities $dN(b)/d\eta \propto N_{part}(b)$ proportional to the number of participants (“wounded” nucleons)

$$N_{part}(b) = \int d^2 \mathbf{x}_\perp [T_A(\mathbf{x}_\perp + \mathbf{b}) + T_A(\mathbf{x}_\perp - \mathbf{b})] \times \left(1 - e^{-\sigma_{NN} T_A(\mathbf{x}_\perp)}\right). \quad (10)$$

Here the inelastic nucleon-nucleon cross section is $\sigma_{NN} = 42$ mb at $\sqrt{s_{NN}} = 200$ GeV (RHIC) and 70 mb at $\sqrt{s_{NN}} = 2.76$ TeV (LHC), and we match the “gluon” multiplicity $dN/d\eta$ to the observed charge particle dN/dy via setting $dN(b=0)/d\eta = 1100$ (Au+Au) and 2400 (Pb+Pb). For the transverse density *profile*, on the other hand, we use the same binary collision distributions as for jets. This choice is motivated by a classical Yang-Mills (“color glass condensate”) calculation[23] that found eccentricities at early times to be much closer to binary collision eccentricities than to wounded nucleon eccentricities.

The initial conditions above are more general than they may appear at first sight. Due to scalings[24] of the transport equation (9), a single transport solution contains the answer to a whole class of *equivalent* problems with scaled initial conditions, cross sections, and particle properties. For example, one can freely increase the initial density provided cross sections are reduced in inverse proportion to keep the mean free path the same. The initial temperature can also be rescaled together with particle masses (in fact for our massless quanta, T_0 does not influence the density evolution at all).

Though in principle the transport provides an ensemble of evolving scattering centers, here we solely use density information to calculate energy loss. Technically this is very similar to employing ideal or viscous hydrodynamics for the medium evolution. We plan to explore different bulk dynamics models in the future.

III. RESULTS

Below we focus on two basic high- p_T observables for neutral pions at midrapidity, the nuclear suppression factor R_{AA} and the momentum anisotropy (elliptic flow) $v_2 = \langle \cos 2\phi \rangle_{p_T}$. Only energy loss is considered, i.e., contributions by the radiated gluons to the final spectrum and feedback on the bulk medium due to the jet were ignored. This is a good approximation at sufficiently high p_T .

We consider **four scenarios** based on i) whether the medium is only undergoing Bjorken expansion (“1D” as in [9, 10]) or transverse expansion as well (“3D”); and ii) whether average energy loss $\langle \Delta E \rangle$ is used or the stochastic $\Delta E(z)$.

Before we turn to results for RHIC and LHC, it is illustrative to compare these scenarios for gluon jets of *fixed* initial energy in $Au + Au$ at RHIC with $b = 8$ fm. Every aspect of the calculation (such as production points with binary collision profile, uniform angles in azimuth, etc) is as discussed above except that the gluon jets all start out with energy $E_0 = 20$ GeV. Figure 2 shows the final jet energy distribution after energy loss. The first obvious feature is that in both 1D and 3D scenarios, stochastic energy loss gives a broader energy loss distribution than using the average $\langle E \rangle$. This is natural since averaging reduces fluctuations in general. Given that parton spectra are convex at high p_T , more fluctuation with stochastic energy loss should result in weaker nuclear suppression (higher R_{AA}), for the same α_s .

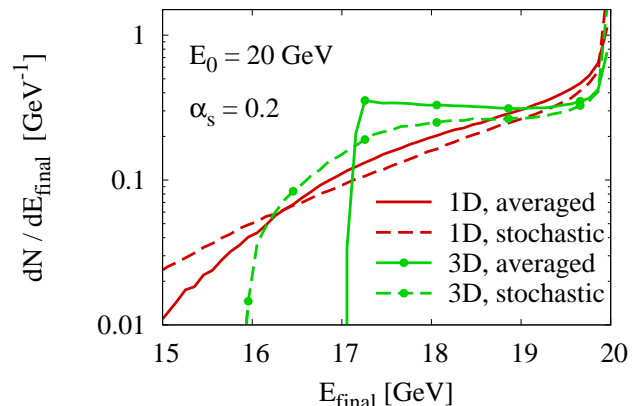


FIG. 2: Final energy distribution for gluon jets of fixed initial energy 20 GeV in four scenarios (see text) for $Au + Au$ at $\sqrt{s_{NN}} = 200$ GeV with $b = 8$ fm, using averaged or stochastic energy (solid vs dashed) with or without transverse expansion for the medium (lines without symbols vs lines with symbols). All distributions are normalized to unit area. In the 3D case, the medium evolution was computed using the parton transport MPC[7].

Another noticeable feature in Fig. 2 is that the distribution is *narrower* with transverse expansion (3D) than with longitudinal expansion only (1D). This is a result of the interplay between energy loss and transverse expansion of the density profile. In the “frozen” 1D case, largest energy loss occurs for jets that start spatially out of plane and move through the center of the collision zone along the long axis of the almond-shaped transverse profile. With transverse expansion, however, the situation is the opposite. Largest energy loss occurs for jets that start in-plane and move along the *initially* shorter axis of the almond. Because the medium expands faster in the in-plane direction, by the time these jets cross the center,

the spatial eccentricity largely disappears (near the collision center the elongation is actually in-plane already but the tail of the density distribution away from the center still keeps traditional eccentricity $\varepsilon = \langle y^2 - x^2 \rangle / \langle x^2 + y^2 \rangle$ positive). The low-energy side of the final jet energy distribution in Fig. 2 cuts off more quickly in the 3D case because the probability for hard scattering (forming a jet) at the edge of the collision zone drops much sharper in-plane than out-of-plane.

Rapid transformation of the collision zone towards a more axially symmetric shape also reduces the energy loss difference between jets crossing through the collision center in-plane vs out-of plane (what in-plane jets miss in opacity while approaching the center they make up for while leaving it, and vice versa), which explains why the energy loss distribution is much flatter in the transversely expanding case.

A. Nuclear suppression in Au+Au at RHIC

Figure 3 shows our results for neutral pion R_{AA} at RHIC, for fixed $\alpha_s = 0.29$ for all four scenarios. With stochastic energy loss the suppression is noticeably weaker, as expected for “upward curving” parton spectra at high p_T . Quite interestingly, realistic transverse expansion significantly enhances jet quenching. This is a generic feature of GLV energy loss coming from the $(1 - \cos)$ interference term in (1). Scatterings at large z induce larger energy loss (cf. Fig. 1), and with a transversely expanding density profile there is higher chance to scatter further away from the production point than in the transversely frozen case.

Unfortunately, without precise control over α_s , R_{AA} alone cannot differentiate between our four scenarios. As shown in Fig. 4, after a slight tuning of α_s to reproduce the suppression in central collisions, differences in R_{AA} largely disappear. We need $\sim 10 - 20\%$ higher α_s with fluctuating energy loss than with the path-averaged one, while $\sim 10 - 15\%$ lower α_s with transverse expansion than without it.

B. Elliptic flow in Au+Au at RHIC

Luckily, p_T -differential elliptic flow turns out to be a much more sensitive probe of the medium evolution and energy loss treatment. Figure 5 shows our results for neutral pion $v_2(p_T)$ in $Au + Au$ at $\sqrt{s_{NN}} = 200$ GeV at RHIC, for fixed $\alpha_s = 0.29$ in all four scenarios. We find that, especially in more peripheral $b = 8$ fm collisions, stochastic energy loss gives smaller elliptic flow both with and without transverse expansion than average energy loss. This is in line with the weaker nuclear suppression for the stochastic case shown in Fig. 3.

On the other hand, transverse expansion *reduces* elliptic flow, and at the same time also gives *smaller* R_{AA} as we have seen in the previous Section. This may seem

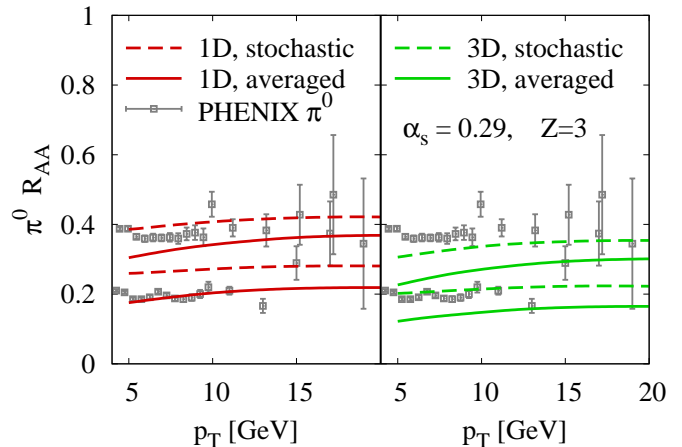


FIG. 3: Neutral pion R_{AA} in $Au + Au$ at $\sqrt{s_{NN}} = 200$ GeV at RHIC with impact parameters $b = 3$ fm and 8 fm (lower pair of lines vs upper pair of lines, respectively, in both panels) calculated in four different scenarios with GLV energy loss (see text). *Left panel*: transversely frozen density profiles. *Right panel*: realistic transverse expansion modeled with parton transport MPC[7]. *Dashed curves* were obtained with fluctuating energy loss, while *solid curves* with averaged energy loss along the jet path. Data[25] from PHENIX (boxes) are also shown for comparable centralities 0-10% and $\approx 30\%$ to guide the eye.

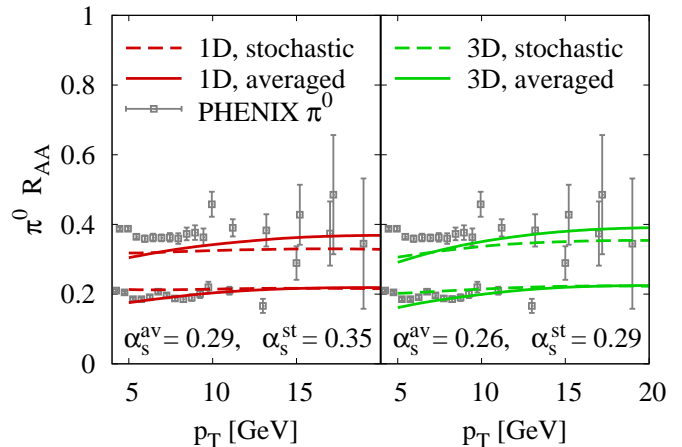


FIG. 4: Same as Fig. 3 but with α_s tuned in all four scenarios to reproduce R_{AA} in nearly central ($b = 3$ fm) collisions.

counter-intuitive at first, but it is also a feature of GLV energy loss. Because the interference term in (1) biases against early scattering in the medium, a jet parton loses more energy if it scatters further away from the production point, which also means the scattering is later in time. Compared to the transversely “frozen” 1D scenario, transverse expansion gives at later times higher densities away from the center, so there is more quenching, but at the same time the medium also rapidly becomes more azimuthally symmetric, so the elliptic flow

response is weaker.

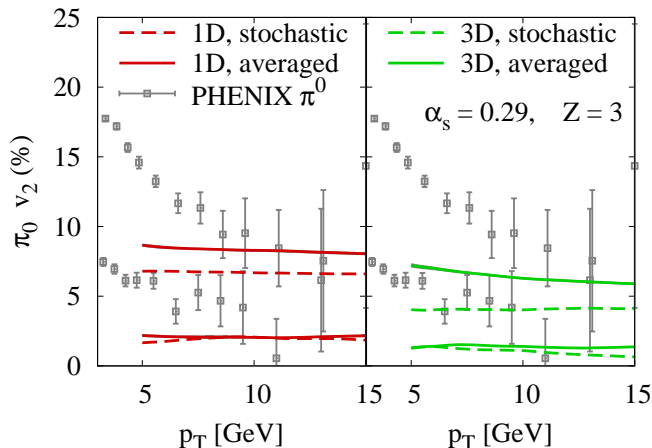


FIG. 5: Neutral pion v_2 in $Au + Au$ at $\sqrt{s_{NN}} = 200$ GeV at RHIC with impact parameters $b = 3$ fm and 8 fm (lower pair of lines vs upper pair of lines, respectively, in both panels) calculated in four different scenarios with GLV energy loss (see text). *Left panel*: transversely frozen density profiles. *Right panel*: realistic transverse expansion modeled with parton transport MPC[7]. *Dashed curves* were obtained with fluctuating energy loss, while *solid curves* with averaged energy loss along the jet path. Data[26] from PHENIX (boxes) are also shown for comparable centralities 0-10% and $\approx 30\%$ to guide the eye.

The reduction of v_2 in the 3D case is manifest even after α_s is tuned to reproduce R_{AA} in central collision, as shown in Fig. 6. For both averaged energy and stochastic energy loss, v_2 is reduced by $\approx 40\%$ (nearly half!) at high $p_T \sim 10 - 15$ GeV due to transverse expansion. Similar reduction is present at LHC energies as we discuss in Section III D. In the more realistic “3D” scenario with both transverse and longitudinal expansion, both averaged and stochastic energy loss give about the same $v_2(p_T)$ at high p_T for both centralities we studied.

C. Nuclear suppression in Pb+Pb at the LHC

Now we turn to results for Pb+Pb at LHC energies. For the nuclear suppression, we find the same generic features as in Au+Au at RHIC: i) medium evolution with transverse expansion gives stronger suppression (smaller R_{AA}) than the transversely “frozen” scenario, and ii) stochastic energy loss gives less suppression than the path-averaged (ΔE).

Figure 7 shows our results for neutral pion R_{AA} in Pb+Pb at $\sqrt{s_{NN}} = 2.76$ TeV at the LHC, after α_s has been adjusted to reproduce the suppression measured around $p_T \sim 8$ GeV. At LHC energies we only computed the transport evolution for $b = 8$ fm collisions, therefore in the 3D scenarios we adjust α_s to R_{AA} measurements for $\approx 30\%$ centrality ($b = 8$ fm) instead of 0 – 10% central collisions ($b \approx 3$ fm). We generally find that in all

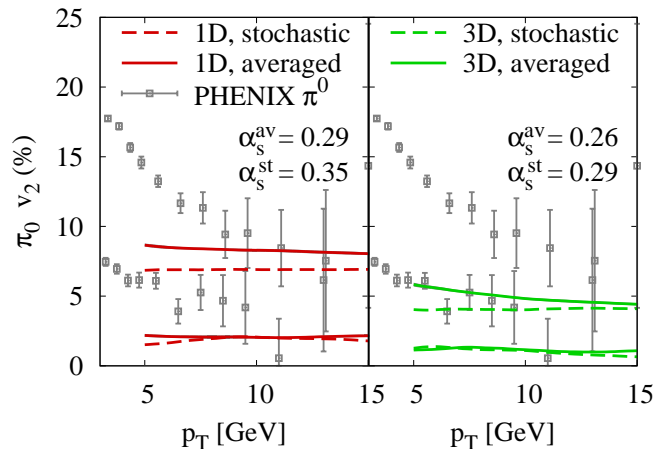


FIG. 6: Same as Fig. 5 but with α_s tuned in all four scenarios to reproduce R_{AA} in nearly central ($b = 3$ fm) collisions.

cases studied stochastic energy loss gives somewhat flatter R_{AA} than a computation using the average energy loss. From our fixed-coupling calculation, R_{AA} curves rise with p_T slower than the trend in the data. Incorporation of running $\alpha_s(Q^2)$, as was done, e.g., in [28], should yield better agreement.

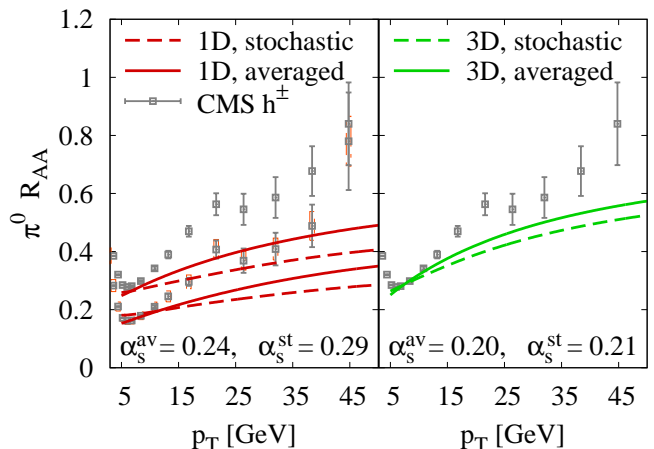


FIG. 7: Neutral pion R_{AA} in $Pb + Pb$ at $\sqrt{s_{NN}} = 2.76$ TeV at the LHC with impact parameters $b = 3$ fm (left panel only) and 8 fm (both panels) calculated in four different scenarios with GLV energy loss (see text). *Left panel*: transversely frozen density profiles. *Right panel*: realistic transverse expansion modeled with parton transport MPC[7]. *Dashed curves* were obtained with fluctuating energy loss, while *solid curves* with averaged energy loss along the jet path. Charged hadron data[27] from CMS (boxes) are also shown, scaled to comparable centralities 0-10% and $\approx 30\%$, to guide the eye.

We need somewhat larger α_s values to match the observed suppression at RHIC than to reproduce suppression at the LHC (Fig. 4 vs Fig. 7), i.e., the medium at the LHC appears somewhat less opaque to jets than extrapolation based on RHIC data would suggest. Our results

thus qualitatively reinforce the findings in [29], although we see about twice as large an effect. In our transversely static (1D) scenarios the ratio of LHC to RHIC effective couplings is about $\alpha_s^{LHC}/\alpha_s^{RHIC} \approx 0.8$, while with transversely expanding medium the ratio is somewhat lower, $\alpha_s^{LHC}/\alpha_s^{RHIC} \sim 0.75$.

D. Elliptic flow in Pb+Pb at the LHC

Finally we demonstrate that with GLV energy loss the striking reduction of high- p_T elliptic flow seen at RHIC energies for transversely expanding media also occurs at LHC energies. Figure 8 shows our results for neutral pion $v_2(p_T)$ in $Pb + Pb$ at $\sqrt{s_{NN}} = 2.76$ TeV at the LHC, again after α_s has been adjusted to reproduce $R_{AA}(p_T \sim 8 \text{ GeV})$. We only find a very small reduction of elliptic flow due to stochastic energy loss compared to using the average $\langle \Delta E \rangle$ along the jet path. The difference between transversely “frozen” evolution and full 3D expansion, however, is even larger than in Fig. 6 for RHIC collisions. By $p_T = 5$ GeV, v_2 is reduced by more than half, and above $p_T = 15$ GeV by more than two-thirds, irrespectively of whether we use average energy loss or the stochastic one.

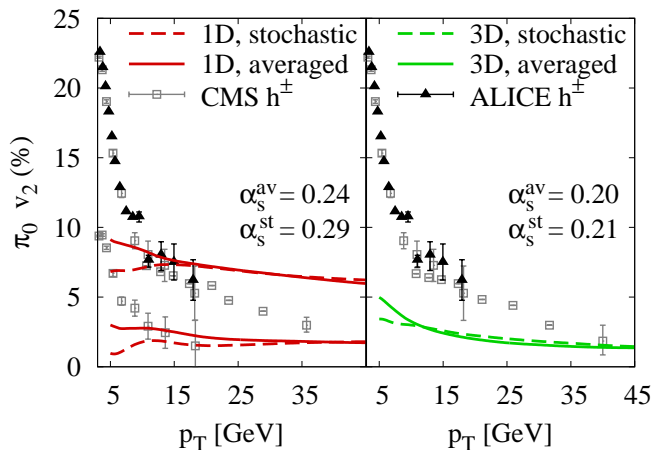


FIG. 8: Neutral pion $v_2(p_T)$ in $Pb + Pb$ at $\sqrt{s_{NN}} = 2.76$ TeV at the LHC with impact parameters $b = 3$ fm (left panel only) and 8 fm (both panels) calculated in four different scenarios with GLV energy loss (see text). *Left panel:* transversely frozen density profiles. *Right panel:* realistic transverse expansion modeled with parton transport MPC[7]. *Dashed curves* were obtained with fluctuating energy loss, while *solid curves* with averaged energy loss along the jet path. Charged hadron data[30, 31] from CMS (boxes) and ALICE (triangles) are also shown, scaled to comparable centralities 0-10% and $\approx 30\%$, to guide the eye.

IV. CONCLUSIONS

In this work we investigated nuclear suppression and elliptic flow in $A + A$ reactions at RHIC and the LHC using Gyulassy-Levai-Vitev (GLV) energy loss with the covariant transport model MPC[7] for the bulk medium. We compared calculations with transversely “frozen” density profiles (as in [9, 10]) to calculations with realistic transverse expansion, and also studied the difference between path-averaged (deterministic) energy loss and stochastic energy loss that fluctuates depending on the location of the scattering center that interacts with the jet parton.

Our most striking finding is that, at both RHIC and LHC, realistic transverse expansion strongly suppresses elliptic flow at high p_T compared to calculations with longitudinal Bjorken expansion only. We argue that this is a generic feature of GLV energy loss, coming from interference bias against early rescattering in the medium.

We also find that transverse expansion enhances high- p_T suppression, while energy loss fluctuations in the stochastic case lead to weaker suppression and smaller elliptic flow. However, unlike the strong reduction of elliptic flow with transverse expansion, these latter effects nearly disappear once calculations are adjusted to reproduce R_{AA} in central collisions.

Though our calculation lacks a few relevant effects such as elastic energy loss and multi-gluon emission, the results do suggest that GLV energy loss will have difficulty with the simultaneous description of nuclear suppression and elliptic flow at RHIC and the LHC. In view of the $R_{AA}(\phi)$ challenge posed for perturbative QCD energy loss in a recent compilation[11] by PHENIX, we believe it is imperative to test our findings with more full-fledged GLV implementations[9, 10], and also other bulk evolution models (such as hydrodynamics).

Acknowledgments

We thank A. Buzzatti, I. Vitev, M. Gyulassy and W. Horowitz for stimulating discussions. This work was supported by the US DOE under grant DE-PS02-09ER41665. D.S. was partially supported by the JET Collaboration (DOE grant DE-AC02-05CH11231).

Appendix A: The energy loss integral I

Here we discuss how Eq. (7) is obtained. Substituting (1) and (6) into (2) leaves one with five integrals to do. Axial symmetry $d^2\mathbf{q} d^2\mathbf{k} dx = (\pi/2) d(q^2) d(k^2) d\varphi dx$ reduces these to four, and with dimensionless variables

$$\kappa = \frac{k}{\mu}, \quad \xi = \frac{q}{\mu}, \quad \epsilon = \frac{E}{\mu}, \quad b = \frac{z}{\tau}, \quad (\text{A1})$$

and $u = (\mathbf{k} - \mathbf{q})^2/\mu^2 = \kappa^2 + \xi^2 - 2\kappa\xi \cos \phi$, we have

$$I(b, \epsilon) = \int_0^{3\epsilon} d(\xi^2) \int_0^\pi \frac{d\phi}{\pi} \int_0^\epsilon d\kappa \int_{x_{\min}}^1 dx \frac{2\xi \cos \phi}{(\xi^2 + 1)^2 u} \times \left(1 - \cos \frac{ub}{x}\right) \quad (\text{A2})$$

where the lower limit on the x integral is $x_{\min} = \max(1, \kappa)/\epsilon$. The innermost integral is doable with the help of

$$\int dx \cos \frac{\alpha}{x} = x \cos \frac{\alpha}{x} + \alpha \text{Si} \frac{\alpha}{x} \quad (\text{A3})$$

where Si is the sine integral function. The remaining three integrals can be evaluated numerically (at some expense because the integrand is oscillatory).

For a numerically easier approximate result, one may momentarily ignore the upper bound (6) on q . With new variable $\mathbf{q} \rightarrow \mathbf{Q} = (\mathbf{k} - \mathbf{q})/\mu$, \mathbf{Q} is then unrestricted and we have, again in polar coordinates $d^2\mathbf{Q} d^2\mathbf{k} dx = (\pi/2) d(Q^2) d(k^2) d\phi dx$,

$$I(b, \epsilon) \rightarrow \int_{1/\epsilon}^1 dx \int_0^\infty \frac{du}{u} \left(1 - \cos \frac{ub}{x}\right)$$

$$\times \int_0^{x\epsilon} d\kappa \int_0^\pi \frac{d\phi}{\pi} \frac{2(\kappa - Q \cos \phi)}{(\kappa^2 + u - 2\kappa Q \cos \phi + 1)^2}. \quad (\text{A4})$$

The ϕ and κ integrals evaluate to

$$g(u, x\epsilon) = \frac{1}{1+u} - \frac{1}{\sqrt{x^2\epsilon^2 + 2x\epsilon(1-u) + (1+u)^2}} \quad (\text{A5})$$

Restoring now an approximate ϕ -averaged upper limit on Q^2 , $Q^2 = u \sim \kappa^2 + \xi^2 \leq x^2\epsilon^2 + 3\epsilon < 4x\epsilon^2$ gives the simpler 2D integral

$$I_{2D}(b, \epsilon) = \int_{1/\epsilon}^1 dx \int_0^{4x\epsilon^2} \frac{du}{u} \left(1 - \cos \frac{ub}{x}\right) g(u, x\epsilon), \quad (\text{A6})$$

which approximates the full result (A2) well in practice provided $E/\mu \gtrsim 10$ (cf. Fig. 1).

-
- [1] A. Drees, H. Feng and J. Jia, Phys. Rev. C **71**, 034909 (2005) [nucl-th/0310044]; J. Jia and R. Wei, Phys. Rev. C **82**, 024902 (2010) [arXiv:1005.0645 [nucl-th]].
- [2] J. Liao and E. Shuryak, Phys. Rev. Lett. **102**, 202302 (2009) [arXiv:0810.4116 [nucl-th]].
- [3] B. Betz and M. Gyulassy, Phys. Rev. C **86**, 024903 (2012) [arXiv:1201.0281 [nucl-th]].
- [4] R. Baier *et al.*, Nucl. Phys. B **483** (1997) 291;
- [5] U. A. Wiedemann, Nucl. Phys. A **690** (2001); C. A. Salgado and U. A. Wiedemann, Phys. Rev. D **68**, 014008 (2003)
- [6] M. Gyulassy, P. Levai and I. Vitev, Nucl. Phys. B **571** (2000) 197; M. Gyulassy, P. Levai and I. Vitev, Nucl. Phys. B **594**, 371 (2001) [nucl-th/0006010].
- [7] D. Molnar and M. Gyulassy, Phys. Rev. C **62**, 054907 (2000); D. Molnar, MPC 1.8.11. This transport code is available at <http://karman.physics.purdue.edu/OSCAR>
- [8] D. Molnar and D. Sun, arXiv:1209.2430 [nucl-th], to appear in Nucl. Phys. A
- [9] A. Buzzatti and M. Gyulassy, Phys. Rev. Lett. **108**, 022301 (2012) [arXiv:1106.3061 [hep-ph]].
- [10] W. A. Horowitz, AIP Conf. Proc. **1441**, 889 (2012) [arXiv:1108.5876 [hep-ph]].
- [11] A. Adare *et al.* [PHENIX Collaboration], arXiv:1208.2254 [nucl-ex].
- [12] S. Wicks, arXiv:0804.4704 [nucl-th].
- [13] M. Gyulassy, I. Vitev, X. -N. Wang and P. Huovinen, Phys. Lett. B **526**, 301 (2002) [nucl-th/0109063].
- [14] S. Wicks, W. Horowitz, M. Djordjevic and M. Gyulassy, Nucl. Phys. A **783**, 493 (2007) [nucl-th/0701063].
- [15] M. Djordjevic and U. Heinz, Phys. Rev. C **77**, 024905 (2008) [arXiv:0705.3439 [nucl-th]].
- [16] T. Renk, Phys. Rev. C **85**, 044903 (2012) [arXiv:1112.2503 [hep-ph]].
- [17] H. L. Lai *et al.* [CTEQ Collaboration], Eur. Phys. J. C **12**, 375 (2000) [hep-ph/9903282].
- [18] M. Gyulassy and X. Wang, Comput. Phys. Commun. **83**, (1994) 307 [nucl-th/9502021]. For gold the radius and thickness are $R = 6.38$ fm and $\delta = 0.535$ fm, while for lead $R = 6.624$ fm and $\delta = 0.549$ fm.
- [19] J. Binnewies, B. A. Kniehl and G. Kramer, Z. Phys. C **65**, 471 (1995)
- [20] D. Molnar and P. Huovinen, Phys. Rev. Lett. **94**, 012302 (2005) [nucl-th/0404065].
- [21] P. Huovinen and D. Molnar, Phys. Rev. C **79**, 014906 (2009) [arXiv:0808.0953 [nucl-th]].
- [22] D. Molnar, arXiv:0806.0026 [nucl-th].
- [23] T. Lappi and R. Venugopalan, Phys. Rev. C **74**, 054905 (2006) [nucl-th/0609021].
- [24] D. Molnar and M. Gyulassy, Phys. Rev. C **62**, 054907 (2000) [nucl-th/0005051].
- [25] A. Adare *et al.* [PHENIX Collaboration], Phys. Rev. Lett. **101**, 232301 (2008) [arXiv:0801.4020 [nucl-ex]]. For $\approx 30\%$ centrality, we plot as a simple estimate the arithmetic mean of R_{AA} measurements in the 20 – 30% and 30 – 40% centrality bins.
- [26] A. Adare *et al.* [PHENIX Collaboration], Phys. Rev. Lett. **105**, 142301 (2010) [arXiv:1006.3740 [nucl-ex]]. For $\approx 30\%$ centrality, we plot as a simple estimate the arithmetic mean of v_2 measurements in the 20 – 30% and 30 – 40% centrality bins.
- [27] S. Chatrchyan *et al.* [CMS Collaboration], Eur. Phys.

- J. C **72**, 1945 (2012) [arXiv:1202.2554 [nucl-ex]]. For $\approx 0-10\%$ and $\approx 30\%$ centrality, we plot as simple estimates the arithmetic means of R_{AA} measurements in the $0-5\%$ and $5-10\%$ centrality bins, and $10-30\%$ and $30-50\%$ centrality bins, respectively.
- [28] A. Buzzatti and M. Gyulassy, [arXiv:1210.6417 [hep-ph]].
- [29] B. Betz and M. Gyulassy, Phys. Rev. C **86**, 024903 (2012) [arXiv:1201.0281 [nucl-th]].
- [30] S. Chatrchyan *et al.* [CMS Collaboration], Phys. Rev. C **87**, 014902 (2013) [arXiv:1204.1409 [nucl-ex]]; S. Chatrchyan *et al.* [CMS Collaboration], Phys. Rev. Lett. **109**, 022301 (2012) [arXiv:1204.1850 [nucl-ex]]. To estimate $\approx 0-10\%$ and $\approx 30\%$ centralities, we averaged v_2 measurements in the $0-5\%$ and $5-10\%$ centrality bins, and $25-30\%$ and $30-35\%$ centrality bins, respectively ($20-30\%$ and $30-40\%$ for the high- p_T data set).
- [31] B. Abelev *et al.* [ALICE Collaboration], Phys. Lett. B **719**, 18 (2013) [arXiv:1205.5761 [nucl-ex]]. To estimate $\approx 30\%$ centrality, we averaged v_2 data in the $20-30\%$ and $30-40\%$ centrality bins.
- [32] Roughly speaking, $R_{AA} \approx [R_{AA}(\phi=0) + R_{AA}(\phi=\pi/2)]/2$, while $v_2 \approx [R_{AA}(\phi=0) - R_{AA}(\phi=\pi/2)]/(4R_{AA})$.
- [33] Boldly applying at temperatures $T \sim 150-700$ MeV accessible at RHIC and the LHC perturbative quark-gluon plasma expressions for density and Debye mass,

$$\frac{n}{T^3} = (16 + 9N_f) \frac{\zeta(3)}{\pi^2}, \quad \frac{\mu}{gT} = \sqrt{1 + \frac{N_f}{6}},$$

$\mu(T(n))$ in a pure gluon plasma ($N_f = 0$) is not that different from a plasma with light quarks ($N_f \approx 2-3$) because the N_f dependences largely compensate each other.

- [34] With the z axis along the beam direction,

$$y = \frac{1}{2} \ln \frac{E + p_z}{E - p_z}, \quad \eta = \frac{1}{2} \ln \frac{t + z}{t - z}$$